Real-time lateral stability and steering characteristic control using non-linear model predictive control

Wian Botes[a], Theunis R. Botha[b*], P. Schalk Els[c]

[a,b,c] Vehicle Dynamics Group, University of Pretoria, co Lynwood and Roper Street, Hatfield, Pretoria, 0002, South Africa

[a] wian.botes@tuks.co.za, [b*] theunis.botha@up.ac.za, [c] schalk.els@up.ac.za

Abstract

This paper presents a non-linear integrated control strategy that primarily focusses maintaining vehicle lateral stability using active front steering (AFS) and differential braking (DB). The proposed control strategy utilises a non-linear model predictive controller to improve lateral stability. A stable linear reference model is used for reference generation. By including the understeer gradient in the reference model, different kinematic responses are obtained from the controlled vehicle. The prediction model utilises the road-friction estimate to create dynamic stability constraints that includes roll-over and sliding of the vehicle. The design of the model predictive controller allows easy activation of different control actuators and dynamic modification to the control behaviour. The control methodology is validated using MATLAB/Simulink and a validated MSC ADAMS model. A sensitivity analysis is conducted to identify the susceptibility of the control strategy to various parameters and states.

Keywords: non-linear model predictive control, integrated control, advanced driver assist system, lateral stability, sideslip angle control.

1 Introduction

A survey from the National Highway Traffic Safety Administration (2015) showed that 94% of crashes across the United States are a result of human-related causes. Of the 94% human-related errors, 33% are decision-based errors and 11% performance-based errors such as, overcompensation and poor directional control. Examples of human-related and decision-based errors include high speeds in the wrong environmental conditions, overcompensation of steering inputs, and poor directional control. Slick roads, or low traction surfaces, contributes to more than half of the 2% recorded overall environmental crash scenarios. These crash statistics enforce the notion that the average human driver is a significant limiting factor in improving vehicle safety.

Advanced Driver Assist System (ADAS) have become common and popular solutions to improve vehicle instabilities and occupancy safety. Electronic Stability Control (ESC) is such a form of ADAS. ESC first featured on commercial vehicles in 1995. The European Commision (2009) passed a regulation that enforced the mandatory fitment of ESC on all new vehicles as of November 2014. With pressure from regulatory bodies to improve the standard safety equipment in passenger vehicles, the performance testing of existing safety features and the development of new safety features are critical contributions that can be made to improve vehicle and occupant safety. An impact analysis performed on the effectiveness of ESC published by the National Highway Traffic Safety Administration (2007), showed that ESC reduces fatal single-vehicle crashes by 35% for passenger vehicles and 67% for Light Trucks and Vans (LTV). LTVs or Sport Utility Vehicles (SUVs) have significantly higher centres of gravity (CG) compared to standard passenger vehicles. ESC is not only effective in preventing single-vehicle crashes but reduces fatal rollovers by 69% for passenger vehicles and 88% for SUVs. A study published by the European Commision (2018), summarises the effectiveness of different ADAS strategies. In this summary, different studies conducted in different

countries around the world showed a significant reduction in fatal and non-fatal crash statistics for vehicles equipped with ESC when compared to vehicles without ESC. A 32% reduction in crashes are observed for wet driving conditions and a 38% reduction in crashes were observed for snowy conditions. Although these technologies show a significant improvement in instability mitigation, a large margin for improvement remains.

Apart from environmental conditions, single performance-based ADAS strategies can also cause vehicle instabilities. Cronjé and Els (2010) mentions that the lateral stability of a vehicle is compromised when using an Active Anti-Rollbar (AARB) system on a single axle.

Sideslip angle is used as a key indicator of the lateral stability of a vehicle (Rajamani, 2012). Unstable vehicles will have a larger sideslip angle when compared to a stable vehicle driving at high or low speed. Thus, simply relying on yaw rate or lateral acceleration as a handling metric may result in an unstable vehicle due to the large sideslip angle required.

To circumvent the single objective ADAS strategies, such as merely improving handling, a multi-objective ADAS strategy can be developed which incorporates handling and stability. By observing different handling and stability metrics simultaneously, this strategy can make the best overall decision for the vehicle. This practice is commonly referred to as Integrated Chassis Control (ICC) (Chen et al., 2016). The theoretical pinnacle for this multi-objective approach is full integration of all systems, sensors and actuators and is called Global Chassis Control (GCC). The goal of this GCC approach is to achieve a fully non-linear and full centralised vehicle ICC system. However, a GCC strategy will be extremely computationally expensive and require a feasible solving rate for real-time implementation.

In this study, a flexible integrated control strategy is proposed to address the aspects of lateral and directional instability while providing means of expansion towards more complex multi-objective ICC strategies.

Many studies have taken advantage of integrated control by utilising Direct Yaw Control (DYC) through differential braking (DB) along with Active Front Steering (AFS) to address lateral instabilities (Cairano et al., 2013, Falcone et al., 2008, Ji et al., 2014, Ren et al., 2016). Independently, these strategies show definitive improvements in vehicle stability in different categories. However, the ideology behind using a combination of these strategies is in the interest of creating an advanced envelope of operation. Differential braking is very effective in lateral stability strategies during high road friction conditions but is undesirable when the friction is extremely low. When the friction conditions are very low, braking reduces the lateral force generation of the tyres even further worsening the lateral instability. By then employing AFS, the lateral force generated by the tyres can then be redirected to improve lateral stability.

Apart from lateral stability, rollover remains a serious safety concern for vehicle platforms with higher located CGs. Yoon et al. (2009) however demonstrated that vehicle rollover can be mitigated using a combined rollover and lateral stability ESC strategy. Many ESC systems are developed for small passenger vehicles and then implemented on SUV's without necessary considering the vehicle rollover. This necessitates the inclusion of roll-over prevention in the ESC implementation.

Throughout literature different optimal control techniques such as Linear Quadratic Regulators (Mirzaei, 2010), Sliding Mode Controllers (Alipour et al., 2014, Ding et al., 2017) and Model Predictive Control (MPC) (Ji et al., 2014, Massera and Wolf, 2015, Ren et al., 2016, Siampis et al., 2015, Zheng et al., 2017) is used to implement these control strategies. A drawback to the abovementioned techniques are the dimensional limitations which restrict the control problems to linear vehicle dynamics or linearised non-linear dynamics. Massera and Wolf (2015), Siampis et al. (2015) and Falcone et al. (2008) all simplify and linearise continuous non-linear vehicle models for control purposes. An anticipated drawback to this

approach is the limited prediction accuracy over a longer preview horizon. Recent research efforts shift focus to the use of Non-Linear strategies such as Non-Linear Model Predictive Control (NMPC) (Siampis et al., 2018, Metzler et al., 2018).

Although NMPC can become more computationally expensive than competitors, this technique and the fidelity in prediction and control aligns with the objectives of reaching a GCC system. Open-source toolkits like ACADO (Quirynen et al., 2015) and FORCESPRO (Zanelli et al., 2020) have significantly reduced the effort required in designing, compiling and embedding non-linear model predictive controllers. In this study, the integrated control strategy will make use of NMPC to implement the lateral and directional stability strategy.

Literature presented by Mirzaei (2010), Siampis et al. (2015), Siampis et al. (2018) and Zheng et al. (2017) constrains the vehicle yaw rate using the maximum anticipated lateral acceleration in an attempt to mitigate lateral instabilities. As previously mentioned, sideslip angle is often a better metric for determining lateral instability of vehicles and will be used to constrain the system in the proposed control strategy similarly to the work of Metzler et al. (2018).

Throughout literature different methods of determining state reference values were used. Mirzaei (2010) employed a piecewise function to obtain the state tracking references for controlled system. Falcone et al. (2008) and Massera and Wolf (2015) opted to use the steady-state response of the prediction models to obtain trajectories for the controlled systems. Ren et al. (2016) utilised a linearised version of the state prediction model to obtain state reference trajectories for the control system while forcing the sideslip trajectory to be zero. The approach of forcing the sideslip angle to be zero should cause unneeded solver and control effort and will not be implemented in the proposed strategy. However, a linearised version of the prediction model will be used to create reference trajectories for the control system to track.

Some of the presented literature (Falcone et al., 2008, Mirzaei, 2010, Massera and Wolf, 2015) neglects the effects of lateral load transfer on the lateral force generation potential. A simple lateral load transfer model will be considered in the proposed solution due to the inherent high roll angles produced by SUVs during cornering.

The main contribution of this study is use of a NMPC model with constraints on several vehicle states to improve stability and safety. The NMPC is also suucesfully solved in real-time using the ACADO open source toolkit. There is also no sensitivity analysis presented in literature to determine the susceptibility of these strategies to variations in input parameters. Therefore, results from a sensitivity analysis focussed on the vehicle parameters and measurement noise will be presented in this paper.

2 Vehicle Models

The proposed NMPC algorithm requires a reference trajectory which is obtained from a stable linear model discussed in 2.1. The NMPC also requires a predictive model to anticipate vehicle behaviour and response to control inputs, these responses are obtained from a non-linear vehicle model discussed in 2.2.

2.1 Linear Vehicle Model

The two wheeled bicycle model is a steady-state 2 degree-of-freedom vehicle model that linearises the lateral tyre forces and neglects weight transfer between wheels. Using a set of carefully selected vehicle parameters, this linear model generates predictable and stable state responses irrespective of the environmental and driving conditions. Abe (2015) provides the following linear state space equations to determine the yaw rate r and sideslip angle β by integrating the following model over time using a steady-state velocity V and steering angle δ.

$$\dot{\mathrm{x}} = \mathbf{A}\mathrm{x} + \mathbf{E}\delta \qquad (1)$$

$$\begin{Bmatrix} \dot{\beta} \\ \dot{r} \end{Bmatrix} = \begin{bmatrix} -\frac{2(C_f+C_r)}{MV} & \frac{2(C_r l_r - C_f l_f)}{MV^2} - 1 \\ \frac{2(C_f l_f + C_r l_r)}{I_{zz}} & \frac{2\left(C_r l_r^2 - C_f l_f^2\right)}{V I_{zz}} \end{bmatrix} \begin{Bmatrix} \beta \\ r \end{Bmatrix} + \begin{Bmatrix} \frac{2C_f}{MV} \\ \frac{2C_f l_f}{I_{zz}} \end{Bmatrix} \delta \qquad (2)$$

Here C_f and C_r is the cornering stiffness of a single front or rear tyre, M is the total vehicle mass, I_{zz} is the yaw inertia of the vehicle and the length from the CG to each axle is l_f and l_r. To modify the behaviour of this model, the understeer gradient U can be used to prescribe the linear steering characteristics of this vehicle model. U is simply described as

$$\mathrm{U} = l_f C_f - l_r C_r \qquad (3)$$

while Gillespie (1992) describes the understeer gradient as

$$\mathrm{U} = \frac{W_r}{2C_r} - \frac{W_f}{2C_f} \qquad (4)$$

Here W_r and W_f is the dynamic weight on the rear and front axles respectively. These formulas describe the sideslip potential of the front and rear axles of the vehicle. Neglecting the change in cornering stiffness, the understeer gradient can be modified to change the steering response of the linear model.

2.2 Non-Linear Vehicle Model

The non-linear model is a double track model that can be obtained by expanding on the linear vehicle model. By adding non-linear tyre models and incorporating load transfer between wheels a more accurate vehicle state prediction can be obtained. An illustration of the non-linear vehicle model's yaw plane is available in **Figure 1**. The figure shows the tyre forces with $F_{fl}, F_{fr}, F_{rl,} F_{rr}$ the lateral tyre forces on each wheel and F_{bl}, F_{br} the total left and right brake force respectively, which is used later in the controller design. This model provides state feedback for the sideslip angle β and yaw rate r when integrated over time. The continuous differential equations for this four-wheel vehicle model are

$$\begin{Bmatrix} \dot{\beta} \\ \dot{r} \end{Bmatrix} = \begin{Bmatrix} \frac{F_{fl}+F_{fr}+F_{rl}+F_{rr}}{MV} - r \\ \frac{l_f(F_{fl}+F_{fr})-l_r(F_{rl}+F_{rr})}{I_{zz}} \end{Bmatrix} \quad (5)$$

The lateral forces are determined using the Magic Formula (Pacejka and Bakker, 1992), the coefficients for this 1989 Pacejka model were exported from a multi-body FTire model (Bosch et al., 2016). Pacejka and Bakker (1992) describe the peak factor D as a function of the friction coefficient μ and the vertical force. Therefore, the tyre model can easily be scaled for different road frictions by simply changing the friction coefficient μ term used in the peak factor.

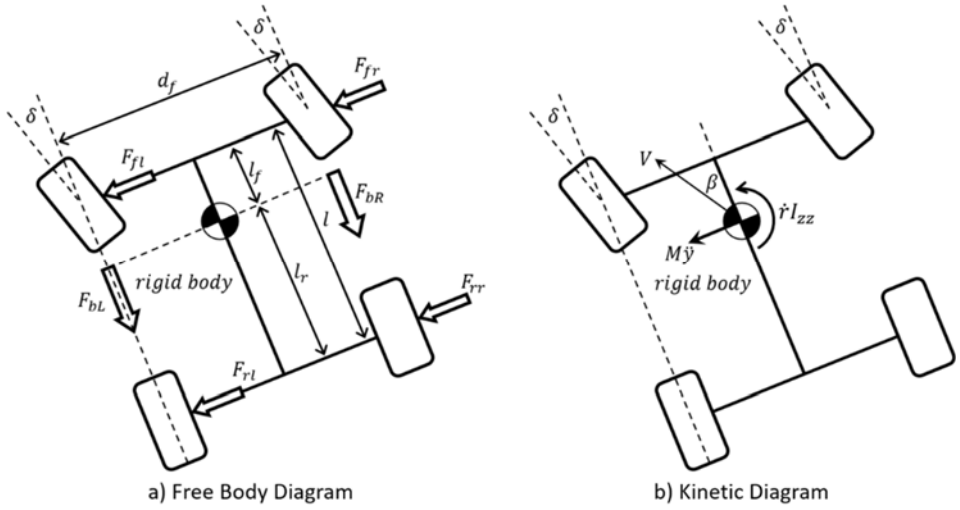

Figure 1 A free-body diagram and kinetic diagram of the yaw plane of a rigid vehicle performing a cornering manoeuvre.

Apart from the vertical force and friction coefficient, the individual sideslip angles of the tyres are required to predict the lateral tyre force using the Magic Formula. The individual tyre slip angles are determined using the following rigid-body kinematics.

$$\beta_{fl} = \tan\left(\frac{Vsin(\beta) + rl_f}{Vcos(\beta) - r(d_f/2)}\right) - \delta \quad (6)$$

$$\beta_{fr} = \tan\left(\frac{Vsin(\beta) + rl_f}{Vcos(\beta) + r(d_f/2)}\right) - \delta \quad (7)$$

$$\beta_{rl} = \tan\left(\frac{Vsin(\beta) + rl_f}{Vcos(\beta) - r(d_f/2)}\right) \quad (8)$$

$$\beta_{rr} = \tan\left(\frac{Vsin(\beta) + rl_f}{Vcos(\beta) + r(d_f/2)}\right) \quad (9)$$

Here d_f is the track width of the vehicle, and l_f and l_r are the perpendicular distances from the CG to the front and rear axles respectively Therefore, the vertical force on each wheel is determined using a simple vehicle rollover model. An illustration of the rigid roll-plane of the vehicle model can be viewed in Figure 2. The lateral load transfer between the inner and outer wheels are determined using a rigid rollover model. This is a simplification as ideally this should be solved by two single order differential equations to obtain the roll velocity and roll angle. However, a rigid roll model is used reduce the complexity of the NMPC model and allow for real-time solutions. The vertical force on each side is obtained using

$$F_{z,L} = \frac{\left(Mg(d_f/2) - Ma_y h_{cg}\right)}{d_f} \quad (10)$$

$$F_{z,R} = Mg - F_{z,L} \quad (11)$$

From (10), a_y is the centripetal acceleration which is calculated as (rV). Individual vertical forces for the front and rear of each side are subsequently determined using the static weight distribution of the vehicle. Therefore, the individual vertical forces are:

$$F_{z,fl} = F_{z,L}\frac{l_r}{l} \quad (12)$$

$$F_{z,fr} = F_{z,R}\frac{l_r}{l} \quad (13)$$

$$(14)$$

$$F_{z,rl} = F_{z,L}\frac{l_f}{l} \qquad (15)$$

$$F_{z,rr} = F_{z,R}\frac{l_f}{l}$$

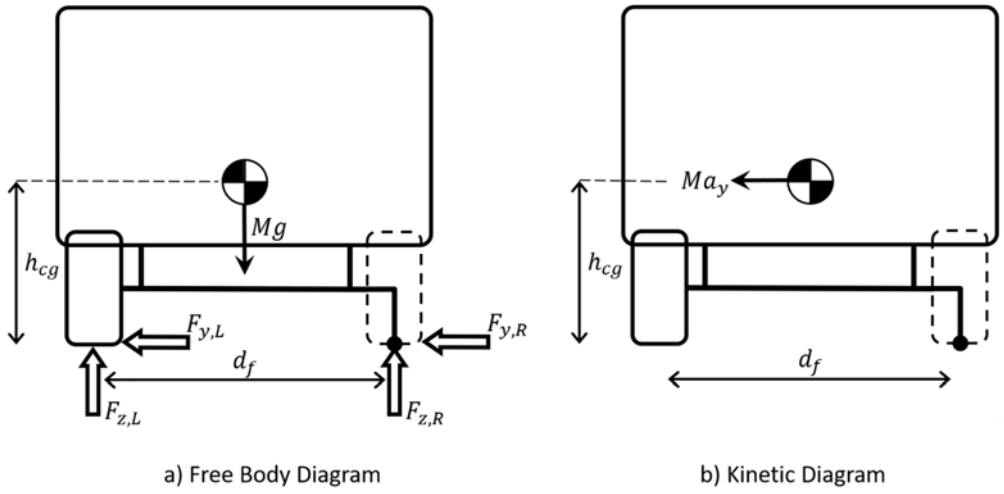

Figure 2 A free-body diagram and kinetic diagram of the roll plane of a rigid vehicle performing a cornering manoeuvre

2.3 Model Parameters and Integration Assumptions

To simulate the model through implicit integration and accurately predict system behaviour, some assumptions regarding inputs to the model and prediction settings are required.

The understeer gradient U is a theoretical indicator of a vehicles steering characteristics with no ideal answer to what the best solution is. Due to the inherent stable nature of an understeering vehicle, the understeer gradient is selected to produce slight understeering state references. The default understeer gradient for this study, unless specified otherwise, is selected as U = -0.1.

For simulation purposes, the road friction coefficient μ is easily obtainable from the simulation configuration settings. During empirical testing and implementation, a complex state estimator or measurement technique is required to obtain real-time friction measurements.

Several coefficient of friction estimators can be found in literature and could be used to address this aspects (Khaleghian, et al, 2017),(Rajamani et al, 2010). Other vehicle parameters are tabulated in Table 1

Table 1: Vehicle properties mass and geometry properties

Vehicle Parameter	Value	Vehicle Parameter	Value
M	$2047kg$	C_f	$2kN/°$
I_{zz}	$2057kg.m^2$	C_r	$1.65kN/°$
l_f	1.55m	d_f	1.49m
l_r	$1.25m$	h_{cg}	$0.4m$

A suitable selection of the prediction time horizon is often based on the natural frequency of the system. However, in vehicle control the steering input to the models are assumed to be constant during the time horizon. However, the requirement of ESC is to improve stability in circumstances where more often severe manoeuvres are performed where the steer angle is non-constant through the manoeuvres. Therefore, the required accuracy of the prediction model over time, will govern the length at which the controller will retain an acceptable prediction fidelity. From Linström et al. (2018) a prediction horizon length of 240 ms will guarantee an R^2 correlation of more than 0.6 for the sideslip angle, 0.8 for the yaw rate and 0.6 for the lateral acceleration when assuming a constant steering rate during severe non-constant manoeuvres. An alternative to either of the steering assumptions are to devise a path predictor to obtain a realistic steering input over the horizon. This, however, requires path and obstacle information which may not be readily available.

3 Non-linear Vehicle Stability Strategy

The proposed non-linear control strategy comprises of different sub-systems. The NMPC controller is exported using the ACADO Toolkit (Quirynen et al., 2015). ACADO employs a standard Least Squares (LSQ) cost functions that can be used for a non-linear controller.

3.1 NMPC Cost Function

The optimisation problem proposed in this strategy is explicit and can be defined using a least squares optimal control problem. The least squares cost function utilised by the ACADO Toolkit is simply:

$$\min_{\substack{x_0,\dots,x_N \\ u_0,\dots,u_{M-1}}} \sum_{k=0}^{N-1} W_{y,k}\|h(x_k,u_k)-\tilde{y}_k\|^2 + \sum_{j=0}^{M-1} W_{u,j}\|u_j\|^2 + W_{y,N}\|h_N(x_N)-\tilde{y}_N\|^2$$

$$\begin{aligned} \text{s.t.} \quad & x_0 = \hat{x}_0 \\ & x_{k+1} = F(x_k,u_k,z_k), \text{ for } k=0,\dots,N-1 \\ & x_k^{lo} \le x_k \le x_k^{up}, \text{for } k=0,\dots,N \\ & u_k^{lo} \le u_k \le u_k^{up}, \text{for } k=0,\dots,N-1 \\ & q_k^{lo} \le q(x_k,u_k) \le q_k^{up}, \text{for } k=0,\dots,N-1 \\ & q_N^{lo} \le q(x_N) \le q_N^{up} \end{aligned} \qquad (16)$$

Here the cost function aims to minimise differential state values (x_k) and control input values (u_j) over the prediction horizon of a length of N steps. The prediction functions h and h_N takes in the state and control values and required reference values ($\tilde{y}_k$ and $\tilde{y}_N$) for each step in the preview horizon. The weighting matrix, $W_{y,k}$ normalises the error between the predicted output state $h(x_k,u_k)$ and trajectory vectors and allow the optimisation results to differ with different weighing values. The weighting matrix $W_{u,j}$ penalises the value of the control input u_j. The optimal control problem requires $\hat{x}_0$, which denotes the current state measurement of the

system and F, which is a discretised ordinary differential equation that is representative of the system behaviour. Finally, the inequality constraints (q), state constraints and control value constraints are constrained by dynamic upper and lower bounds.

3.2 Control Inputs

In order to improve reference tracking the vehicle model has two control inputs namely differential braking and active front steering.

3.1.2 Differential Braking

The lateral and directional stability of the vehicle can be modified using the brakes of the vehicle. Due to the neglected longitudinal dynamics in the tyre models, individual braking forces cannot be modelled and solved using the optimisation problem. In most ESC problems the control output is a yaw moment applied at the vehicle CG. However, since the lateral vehicle dynamics is dependent on the vehicle speed the NMPC model includes the longitudinal deceleration in its formulation. While the yaw moment can be used in the longitudinal acceleration formulation using the absolute value of the moment, it was found that this additional non-linear component significantly affected the solution time. Therefore, a left braking force (F_{bL}) and a right braking force (F_{bR}) is modelled over the tracks of the vehicle in the rearward direction which creates an additional yaw moment about the CG. The yaw acceleration in (5) then simply becomes:

$$\dot{r} = \frac{l_f\left(F_{fl}+F_{fr}\right)-l_r(F_{rl}+F_{rr})+d_f(F_{bL}-F_{bR})/2}{I_{zz}} \qquad (17)$$

Assuming that the only longitudinal forces on the tyres are due to braking, thus no acceleration force is applied, the deceleration of the vehicle is:

$$\ddot{x} = \frac{-F_{bL}-F_{bR}}{M} \qquad (18)$$

The braking forces are subsequently distributed between individual wheels (front and rear) in a lower controller. Using the lateral force and vertical force estimates from the non-linear

vehicle model, the available braking force of each wheel can be estimated. By using the principles of a friction circle, the remaining braking force potential can be calculated as:

$$F_{b,max} = \sqrt{(\mu F_z)^2 - F_y^2} \quad (19)$$

The desired braking force for each side, which is determined by the NMPC, is then split between the front and rear axles using the ratio of maximum available longitudinal force, as:

$$D_R = \frac{F_{b,max\ rear}}{F_{b,max\ front}} \quad (20)$$

$$F_{bfi} = \frac{F_{bi}}{1 + D_R}, i = L\ or\ R \quad (21)$$

$$F_{bri} = F_{bi} - F_{bfi} \quad (22)$$

To preserve directional stability while performing manoeuvres, the algorithm is only allowed to apply the estimated available brake force of each wheel. A drawback to implementing the brake-based torque vectoring in a lower controller is that the prediction model within the NMPC is unaware of the available braking potential of the vehicle. By coupling longitudinal and lateral tyre dynamics the available brake force/torque can be dynamically calculated which should increase the efficiency of the control response even further. This improvement however may come at an increase in computational cost. The brake torques are subsequently determined using

$$T_{bri} = F_{bri} r_w \quad (23)$$

and is applied to the simulation model. Here r_w is the radius of the loaded tyre.

3.2.2 Active Front Steering

The implementation utilised in this paper resembles a steer-by-wire solution where there is a mechanically disconnected steering wheel. The driver and onboard control system can both modify the steering angle simultaneously. This is simply modelled by summing the two

steering inputs and applying the nett steering angle to the vehicle models. The nett steering angle is then simply:

$$\delta = \delta_{driver} + \delta_a \quad (24)$$

It should be noted that the steering input to the reference model is only the desired driver input δ_{driver}.

3.3.2 Enabling and Disabling Control Inputs

A simple method of enabling and disabling the control effort of different control inputs, is by adding activation Booleans to these control values. By simply multiplying the control input sets with their respective Boolean either includes or excludes that effort from the control problem. This implementation is simply defined as:

$$\delta_a = B_{steering}\delta_a \quad (25)$$
$$F_{bR} = B_{braking}F_{bR} \quad (26)$$
$$F_{bL} = B_{braking}F_{bL} \quad (27)$$

Here $B_{steering}$ and $B_{braking}$ are activation Booleans for the active braking and active steering systems. Due to the active set method employed by the quadratic programming solver of ACADO, this addition would not add any significant computational time to find the solution.

3.3 Constraints

The optimisation region of the proposed NMPC strategy is defined by sideslip constraints to ensure lateral stability of the vehicle and a simple rollover constraint to mitigate the risk of vehicle rollovers. Lateral instability is a result of limited traction, creating an oversteer response to driver input. During oversteer, the vehicle is inherently unstable and responds in an unintuitive manner. When the front wheels have low traction, understeer occurs. Understeer can be countered by changing the vehicle speed or increasing the steering effort accordingly. Oversteer however requires unintuitive steering corrections to correct the vehicle response. To observe and mitigate oversteer, constraints are created that restrict the sideslip angle of the vehicle's rear tyres. If the tyres are operated under the friction limit and in the non-linear regime

of the force generation curve, the vehicle in theory should remain stable and predictable. However, the friction limit is highly dependent on several environmental factors and can be simply represented using a simplified single friction coefficient between the tyres and driving surface. Figure 3 shows the lateral tyre force as a function of slip and different friction coefficients.

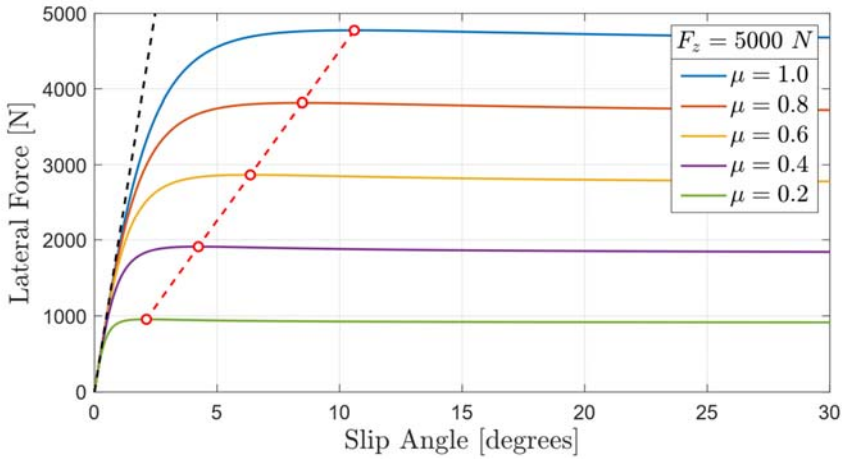

Figure 3 The effect of μ on the lateral force generation of the Magic Formula.

In Figure 3, the lateral force curves for the same loading conditions are plotted for a reducing friction coefficient. The maximum force produced by each condition is indicated using a red marker while the friction limit is therefore defined using a dashed red line. The tyre model used has the maximum lateral force produced at higher slip angles for higher friction coefficients. For optimal tyre performance while maintaining lateral stability, the vehicle should operate as close to the friction limit as possible. To prevent oversteer of the vehicle, rear tyre angles can therefore be constrained to a safe value lower than the friction limit. Constraining the rear slip angles as:

$$\beta_{rl} \leq \pm 7° \mu \quad (28)$$

$$\beta_{rr} \leq \pm 7° \mu \quad (29)$$

allows the control problem some redundancy when finding solutions against or just outside these optimisation boundaries. It should be noted that this is very vehicle characteristic dependent and should be reformulated for a specific tyre and possibility the affect of changing vertical load on each tyre.

Apart from lateral instabilities, the targeted vehicle platform remains susceptible to rollover due to its high centre of gravity, during high-speed manoeuvres. To mitigate rollover of the controlled vehicle, the yaw rate of the vehicle can be constrained using the predicted roll moment of the vehicle. This static rollover threshold prevents the inertial response to the cornering acceleration of the vehicle becoming greater than the weight of the vehicle. The yaw constraint is derived using:

$$Ma_y 2h_{cg} < Mgd_f \tag{30}$$

$$a_y = rV < \pm\frac{gd_f}{2h_{cg}} \tag{31}$$

$$r < \pm\frac{gd_f}{2Vh_{cg}} \tag{32}$$

More complex rollover thresholds can be derived and implemented such as the Zero-Moment Point (Lapapong and Brennan, 2010). The Zero-Moment Point method however requires more vehicle states and parameters which will in turn increase the complexity of the non-linear prediction model.

Slack variables are included in the controller design to improve solver stability and enforce a valid control solution for every control step. The slack variables are included in the control problem using the general form:

$$q_k^{lo} \leq q(x_k, u_k) + s_q \leq q_k^{up} \tag{33}$$

$$s_k^{lo} \leq s_{q_k} \leq s_k^{up} \tag{34}$$

Therefore, three slack variables $[s_{\beta_L}, s_{\beta_R}, s_r]$ are added for the left rear and right rear tyre as well as the yaw rate constraints. The reference function is a simple vector of concatenated states and control input parameters. The reference states are:

$$h(x) = \{\beta, r, F_{bL}, F_{bR}, \delta_a, s_{\beta_L}, s_{\beta_R}, s_r\} \quad (35)$$

$$h_{(x_N)} = \{\beta_N, r_N, V_N\} \quad (36)$$

3.4 Tracking Error Weights

An important factor of the proposed control strategy is the optimisation weights, W_y and W_u in (16), used to bias the cost function. By simply changing the magnitudes completely different control reactions are obtainable. Due to the quadratic form of the cost function, the weight denominator is selected as a soft region that sets the permissibility of error associated to that state or control. When the state or error deviates more than the denominator amount, the incurring cost increases quadratically. In addition to the denominator, the numerator can be selected to add an additional factor of scaling to the cost of the error state or control errors. The first configuration of weights are selected to obtain a stability focussed control response from the optimisation. When disregarding the cost of the state errors, an acceptable deviation from the sideslip angle reference is chosen as one degree while the accepted deviation of the yaw rate is selected as two degrees/second. There are no reference values for the control inputs and therefore there are no cost assigned to the control input tracking errors.

However, the design of the prediction model has an inherent bias towards steering instead of braking. The state sensitivity to braking is determined by obtaining either one of the Jacobian terms with respect to the braking force, which shows an overall low sensitivity of approximately $\pm$3.61e-04. To counteract this effect, a penalty factor is added to the additional steering to allow a more balanced combination of braking and steering effort. The additional weighting factor was determined through recursive testing as 6e4. Finally, the slack variables

weights are selected to significantly scale the cost associated to breaking the set inequality constraints. The weights for the stability focussed controller is given in Table 1.

A second set of weights are presented that drastically changes the behaviour of the control strategy. By adding a penalty factor to the state tracking error weights, the optimisation increases prioritisation of the state reference tracking. The control effort then not only enables the conservation of lateral stability but provides a means of changing the steering characteristics of the vehicle, this controller setting is termed the handling focussed controller. The updated state error tracking weights are provided in Table 3 with unchanged weights the same as Table 2.

Table 2 State Tracking Error and Control Input Weights for the Stability Focussed Lateral Stability Control Strategy

States / Controls	Units	Weights	Value	Units
β	$degrees$	w_β	$\frac{1}{1}$	$\frac{1}{degrees}$
r	$\frac{degrees}{s}$	w_r	$\frac{1}{2}$	$\frac{s}{degrees}$
F_{bL}	N	$w_{F_{bL}}$	$\frac{1}{3500}$	$\frac{1}{N}$
F_{bR}	N	$w_{F_{bR}}$	$\frac{1}{3500}$	$\frac{1}{N}$
δ_a	$degrees$	w_{δ_a}	$\frac{6e4}{3}$	$\frac{1}{degrees}$
s_r	$\frac{degrees}{s}$	w_{s_r}	$1e6$	$\frac{s}{degrees}$
s_{β_L}	$degrees$	w_{β_L}	$1e6$	$\frac{1}{degrees}$
s_{β_r}	$degrees$	w_{β_R}	$1e6$	$\frac{1}{degrees}$

Table 3 State Tracking Error and Control Input Weights for the Handling Focussed Steer Characteristic and Lateral Stability Control Strategy

States / Controls	Units	Weights	Value	Units
β	$degrees$	w_β	$\frac{1e4}{1}$	$\frac{1}{degrees}$
r	$degrees.s^{-1}$	w_r	$\frac{1e4}{2}$	$\frac{1}{degrees}$

4 Simulation Based Validation

A MATLAB/SIMULINK/ADAMS co-simulation is performed using a validated 15 degrees of freedom multi-body dynamics ADAMS vehicle model. This model of the Land Rover

Defender 110 Tdi was created by Cronjé and Els (2010), Thoresson et al. (2009), Uys et al. (2006) and Uys et al. (2006). The ADAMS vehicle includes a semi-active hydro-pneumatic suspension that enables four discrete suspension characteristics. For the purposes of this study a stiff suspension stiffness and damping was used to obtain larger sideslip angle responses from the vehicle. Additionally, the delays pertaining to the control actuation is included in the system. A 100ms delay is expected from the hydraulic brake system while a 200ms delay is expected from the steering actuation.

For this simulation study, only the following instances of lateral instability is used to validate the control strategy.

Limit Oversteer –When the vehicle crosses the limit of friction, instead of responding with predictable vehicle behaviour, severe oversteer of the vehicle occurs. During limit oversteer, the vehicle suddenly loses lateral traction of the rear tyres and enters an uncontrolled slide.

Directional Instability – These instabilities occur when the vehicle does not respond to the driver's steering inputs. An unstable vehicle might continue with a cornering trajectory after the steering was centred.

4.1 Open-loop Constant Steering Angle Manoeuvre

In the following simulations the control strategy was set up in such a way to function as a stability focussed system that only intervenes when instabilities are predicted. This manoeuvre tests the vehicle's limit oversteer with an open-loop step-steer and velocity change. The vehicle initially travels at 30km/h with no steering input, a step steer of 6° is introduced at 5 seconds. At 22 seconds the vehicle is accelerated to a higher speed of 40km/h. The same controller is used with the control Booleans to enable or disable either the steering control and/or braking control for the following results. The set of stability focussed control weights are also used in this simulation. The results presented in **Figure 4** compare different control options to one

another while keeping the controllers and control strategy inputs the same. Firstly, the uncontrolled vehicle (solid grey) is presented as a reference for the controlled vehicle responses. The uncontrolled vehicle is stable during the first half of the manoeuvre, but after the velocity was increased by 10km/h limit oversteer occurred. For all the controlled cases, the vehicle maintained a stable trajectory throughout the manoeuvre. From the yaw rate and sideslip angle responses, a straight exit line is followed once the steering is returned to zero. From these results the controlled vehicle with combined steering and braking controller setting (solid blue) show identical yaw rate and sideslip responses when comparing to the braking only controller settings (dashed orange). The steering only (solid green) controller settings however resulted in a more aggressive control approach with higher control rates. The additional applied steering oscillates during the latter half of the manoeuvre, maintaining the vehicle stability but would provide an unpleasant steering response to the driver.

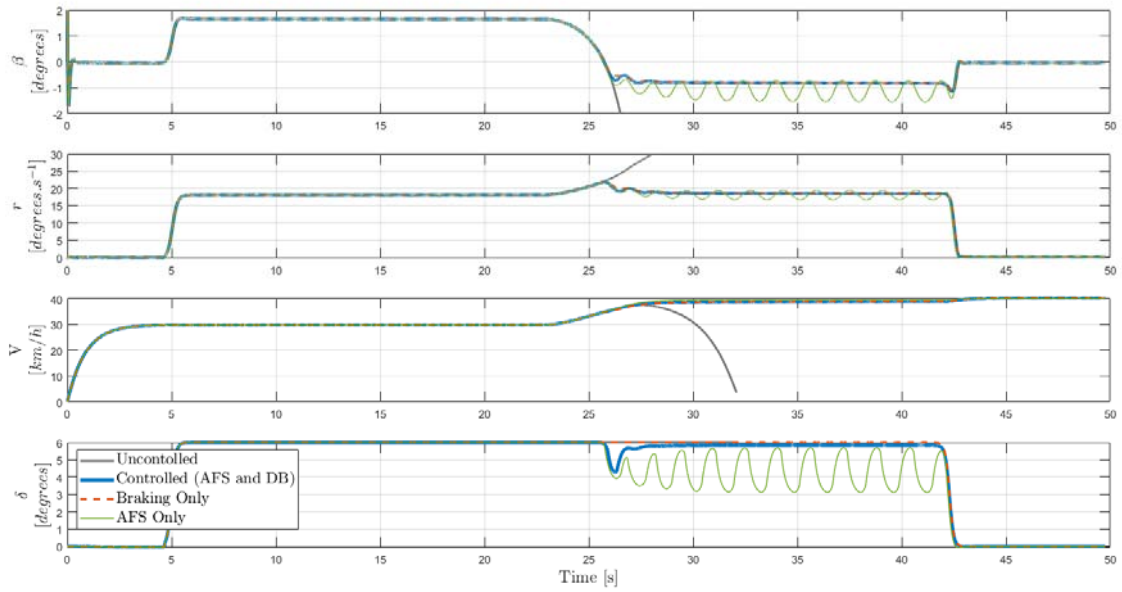

Figure 4 The kinematic results of different constant steering angle manoeuvres performed at 30km/h with a steering angle of 6 degrees and a road friction of $\mu = 0.4$.

The control effort and constrained states responses are presented in **Figure 5**. The control inputs in each simulation only react after the sideslip angle constraints were violated. This allows the vehicle to freely manoeuvre within the envelope defined by the constraints of the controller with intervention only occurring once these constraints are violated. Apart from the oscillatory control of the steering when the braking is disabled, the combined control case and braking only case show critically damped oscillation responses during the reaction phase of the control. The oscillations observed in the control inputs are due to the actuation delays applied to the control signals. If these delays were incorporated into the NMPC model, the oscillations are expected to vanish or at least dissipate greatly. Irrespective of the differences in control responses between simulations, the optimisation iteration count remained similar between the compared simulations indicating similar solution times.

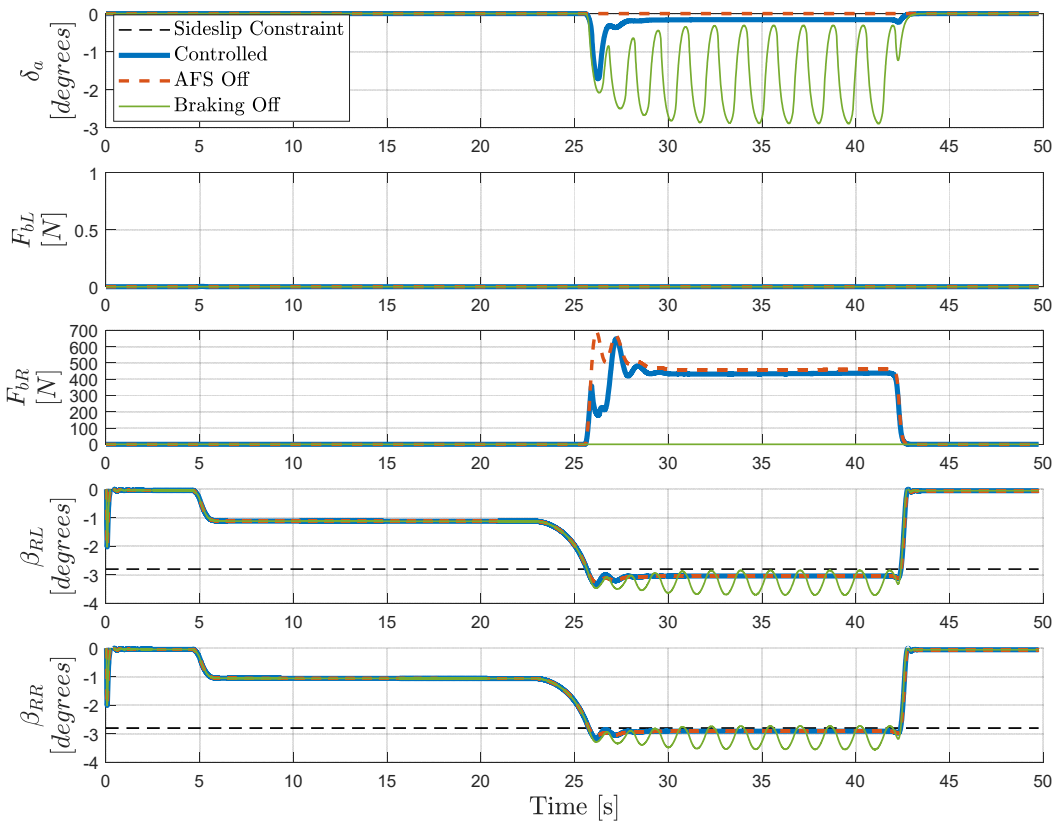

Figure 5 The control input response and constraint values during the constant steering angle manoeuvres.

The number of workset reiterations represent the total number of horizon optimisations that were performed for each control solution. The mean iteration count for all manoeuvres over the latter half of the manoeuvre was 58 iterations compared to the baseline 12. This implies that 46 reiterations were required to find the obtained control solutions. Additionally, it was observed that the objective value and KKT tolerance differences between the steering only and rest of the configurations are higher. Due to the weight associated with steering control and the increase in steering actuation compared to the other simulation configurations, the higher objective and KKT Tolerance is an expected outcome of that specific configuration.

4.2 Open Loop Double Lane Change

In the following simulation results, the stability strategy is evaluated using a transient manoeuvre. The simulation is an open loop double lane change according to ISO 3888:1

(1999). This manoeuvre is generally performed with a closed-loop steering controller or driver, however, to isolate the response of the stability controller from any driver controller the test is performed using open loop. Thus, a steering input is supplied which would be representative of the steering input obtained for a stable vehicle performing the manoeuvre. The test is performed as specified with a coasting velocity, and no additional acceleration forces, as the manoeuvre is performed. Here, the combined braking and handling focussed steering controller setting is used.

Additionally, the tracking weights for sideslip angle and yaw rate are increased to evaluate a more handling focussed steering controller rather than the stability focussed steering controller in the previous simulations. The higher magnitude state error weights promote closer error tracking of the state reference trajectories. This tracking method, in turn, relies on the state reference trajectories and the associated controller inputs such as the understeer gradient U. Whilst keeping the exported controller the same as the previous simulations, the reference models handling characteristics are altered to force the system to exhibit either a more oversteer or understeer characteristics.

The response of the system is presented in **Figure 6**. In these plots, the uncontrolled vehicle response is provided as a reference (solid grey). The uncontrolled vehicle predictably generates large sideslip angle and yaw rate given the initial steering input to the vehicle. However, during the rest of the steering signal, the vehicle remains unresponsive to the driver input, generating a yaw rate and sideslip angle different to what is expected from the steering angle input. The control strategy successfully mitigates all the instabilities experienced with the uncontrolled vehicle. Whenever there is no steering angle applied, the vehicle comes to a stable steady-state between lane changes as well as after the manoeuvre. An example of this is explicitly seen between 10 and 11 seconds. Furthermore, the vehicle scrubs off less velocity during the manoeuvre with the control enabled compared to the uncontrolled case. When

comparing the stability focussed controlled vehicle (solid blue) to the handling focussed controlled vehicles (dashed orange and solid green), a considerable difference in the sideslip and yaw rate responses are noticed for each peak steering angle throughout the manoeuvre.

By comparing the peaks of the handling focussed controlled system and the stability focussed controlled system, more sideslip angle (maximum of four degrees / about 100%) and a higher yaw rate (maximum of five degrees / about 25%) is obtained using the handling focussed control strategy. For the handling focussed systems, a maximum loss of 10km/h or 25% is noticed at the end of the manoeuvre. Ultimately, the increase in yaw rate and sideslip angle does not imply better cornering performance but provides different steering characteristics. When comparing the rms lateral acceleration of the controlled tests, there is no noteworthy difference between configurations.

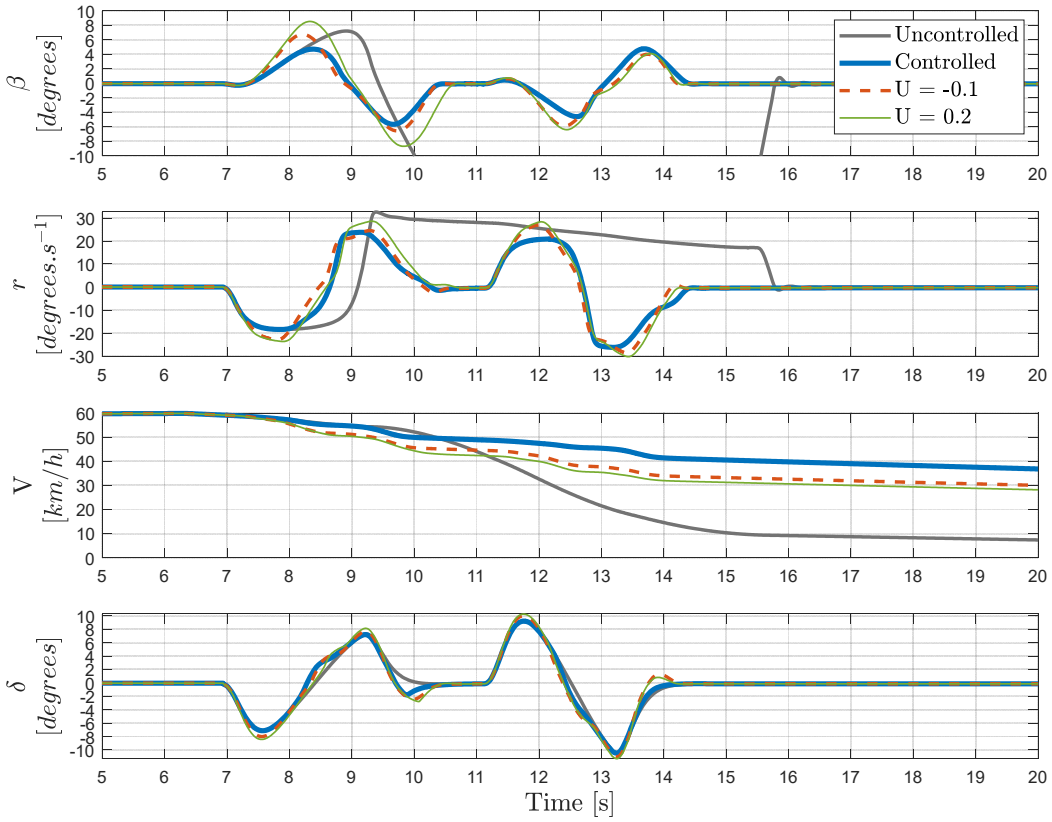

Figure 6 The kinematic response of different controller configurations to a Double Lane Change with an entry speed of 60 km/h, steering modulation of 3δ and a road friction of $\mu = 0.6$.

The control inputs and sideslip constraints for these double lane change simulations are presented in **Figure 7**. As with the previous set of simulations, the stability focused safety system (solid blue) reacts due to the sideslip constraint violations. Control actuation is only applied for the time that the vehicle is outside the constrained region. These control actions of this control setting oppose the inputs from the driver throughout the of manoeuvre. The control efforts of the stability focussed system are noticeably less when comparing to handling focussed systems.

The additional actuation efforts of the handling focussed controller configurations are due to the assisting actuations performed apart from the stabilising actuation effort. Both handling focussed systems assist the driver in turning the vehicle before stabilising the vehicle during the turning of the vehicle. The actuation effort of the more oversteering vehicle (with

understeer gradient U = 0.2) is larger in magnitude and mostly lead when comparing to the more understeering vehicle (U = -0.1). This explains the noticeable differences in sideslip response and the minor difference in yaw rate response. These controller configurations neglect the sideslip constraints and violate them considerably more in comparison to the stability focussed configuration. The magnitude of the violations are justified given the weightings of the state errors and the slack variables.

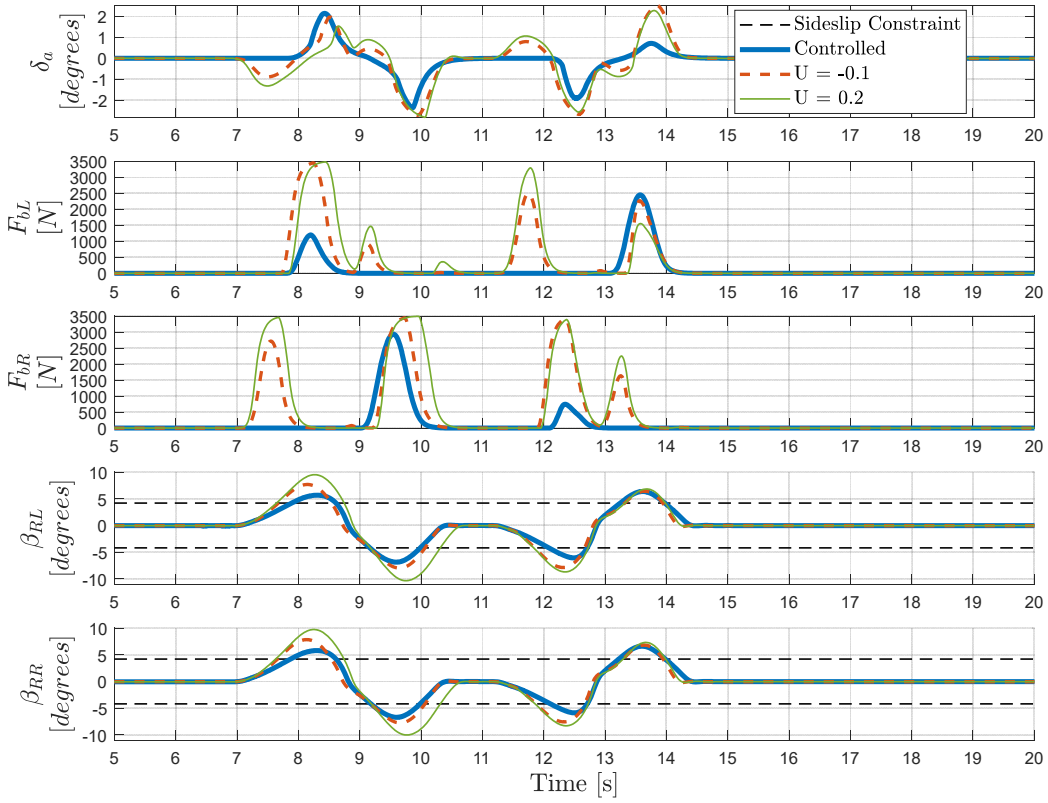

Figure 7 The control input response and constraint values during the double lane change manoeuvres.

There are differences between the objective values and KKT Tolerances of the two handling focussed configuration cases. These differences are attributed to the larger magnitude control effort and larger constraint violations of the more oversteering system. Overall, the optimisation performed similarly to the previous set of steady-state simulations. The peak number of reiterations for these transient manoeuvres are comparable to the previous steady-

state simulations. Comparatively, the peak KKT and objective values of these transient simulations are much higher than the steady-state simulations. This difference is due to the larger weights used in the optimisation.

From a larger set of simulations, the average computational time for the controller that was used in this study is 7.95ms. The average of each simulation is determined using the Simulink Profiler. The profiler however is limited in capability and determines this number as an average. This solution rate allows a control rate of up to of 125 Hz. To be able to statistically quantify the performance of this algorithm, the controller can be embedded in a C++ program to interact with Simulink. From the time varying solver rate obtained in C++, the mean and variance in execution time can be determined.

5 Sensitivity Analysis

To better understand the susceptibility of the control strategy to random variations during implementation, a sensitivity analysis is conducted. Baseline results are obtained using the stability focussed controller settings for this analysis. The set of open-loop constant steer angle manoeuvres that were performed for this investigation can be viewed in Table 4. The following small set of variations were investigated

(1) A 20% shift of the CG towards the front axle on the ADAMS vehicle model.
(2) A 20% shift of the CG towards the rear axle on the ADAMS vehicle model.
(3) A 20% over prediction on the available friction coefficient provided to the control strategy.
(4) A 20% under prediction on the available friction coefficient provided to the control strategy.
(5) A +20% variation in vehicle mass of the prediction model.
(6) A -20% variation in vehicle mass of the prediction model.
(7) Added Noise Thresholds of the available empirical test equipment.
(8) (Similar to 7) with an additional 20% to sideslip angle noise variance.

The expected sensor and platform noise for different control strategy inputs are provided in Table 5. These noise parameters were determined from empirical data captured during the study.

Table 4 The simulated manoeuvres used to perform this sensitivity analysis.

Constant Steer Angle Manoeuvre

Velocity	Steering Angle	Friction
30 km/h	6 degrees	0.4
30 km/h	10 degrees	0.6
40 km/h	10 degrees	0.8
50 km/h	7 degrees	0.6
60 km/h	4 degrees	0.8

Table 5 Standard Deviation of noise thresholds on the required vehicle states and inputs.

Measurement	Noise Variation	Unit
Sideslip Angle	0.051	° rms
IMU Yaw Rate	0.105	$°/s$ rms
GNSS Velocity	0	km/h rms
Steering Angle	0.0553	° rms

5.1 Analysis Results

For this analysis the sensitivity variations of each manoeuvre is compared to a baseline with no parameter variation. The left braking force was inactive during these simulations and was therefore omitted from the results.

A comparison of the results for a single manoeuvre can be viewed in **Figure 8**. In these comparisons, the state outputs and control inputs to the system is directly compared over the entire manoeuvre. The baseline state and control responses are plotted using a dotted black line while the different sensitivity variation responses are plotted using different coloured lines. The most noticeable vehicle state deviations are a result of the friction variations (labelled 3 and 4). The significant deviations of the sideslip angle and yaw rate of the vehicle is a result of the control inputs to the system. When the friction is under-estimated (μ - 20%), more additional steering control and less braking is applied to the vehicle. When the road friction is over-estimated (μ + 20%), the control responses from the strategy is delayed compared to the

baseline responses. This allows the vehicle to assume a larger sideslip angle and yaw rate before the strategy intervenes and prevents the naturally occurring limit-oversteer.

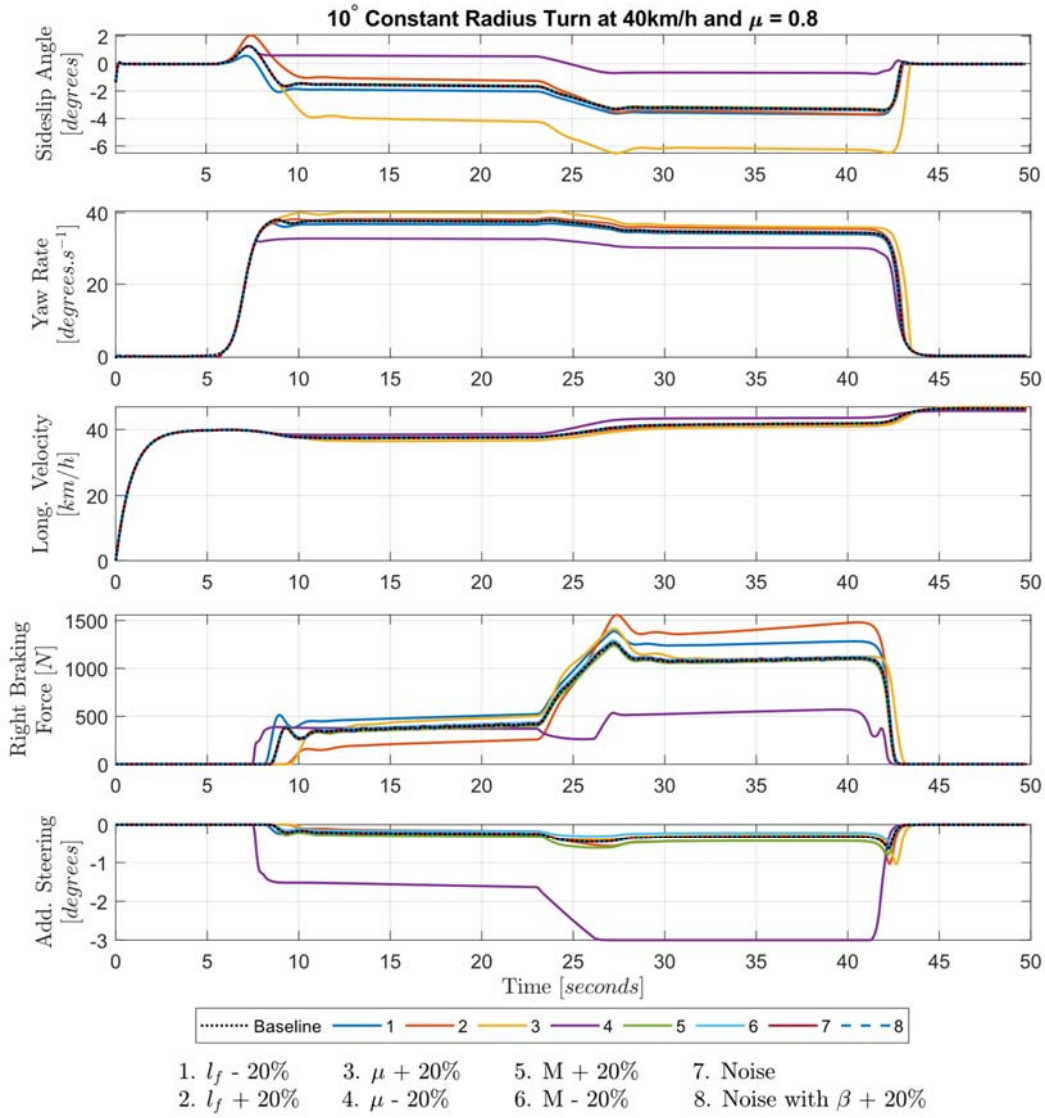

Figure 8 State and control responses of a 10 degree CRT and road friction of 0.8 due to sensitivity variations of different model and strategy parameters.

To better quantify different state and control sensitivity variations over all tests, the state and control deviation from the baseline manoeuvre are obtained. The rms percentage-based deviation from the rms baseline is determined by taking the rms deviation from the baslined and normalising it to the rms value of the baseline response. The percentage-based deviations

are presented in **Figure 9**. The road friction variations (labelled 3 and 4) cause deviations in sideslip angle of larger than 20%, yaw rate deviations of up to 15%, braking control deviation of up to 25% and additional steering deviation of up to 500%. The CG location variations (labelled 1 and 2), show state and control variations smaller than the 20% sensitivity variations induced for the investigation. Additionally, the control strategy shows little sensitivity towards noise on the state measurements. The variations of the prediction model mass and addition of noise on the signal measurements causes negligible state and control deviation of much less than 20%.

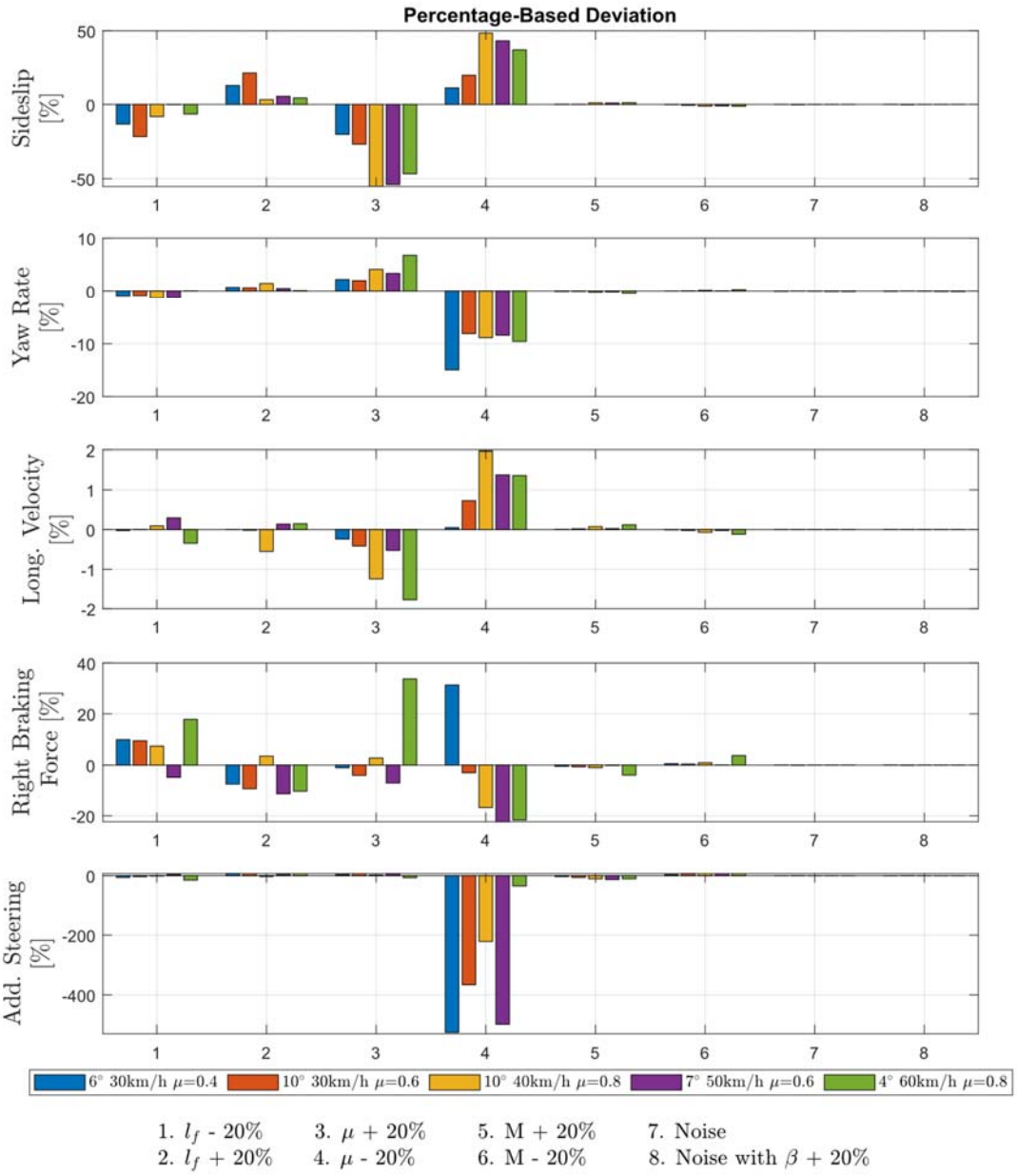

Figure 9 Percentage-Based deviation of the state and control responses due to the variations of the sensitivity parameters when compared to the respective baseline manoeuvre responses.

From this analysis, the friction coefficient estimation and position of the CG is the most sensitive parameters used in the control strategy. All other variations that were tested, showed no significant impact on the state response of the controlled ADAMS vehicle model. The friction estimation forms part of the controller constraints, which indicates to the solver

whether the vehicle is currently within a defined stable state range. When over-predicting the friction potential, the strategy incorrectly allows the vehicle to deviate significantly from the predetermined responses. In a similar way when under-predicting the friction coefficient, the constraints restrict the state response by applying pre-emptive control to vehicle. Pre-emptive control makes the vehicle more predictable and safer but restricts the amount of vehicle handling performance obtainable by the driver.

6 Conclusion

In this paper an integrated control strategy for a traditional SUV was presented. The proposed strategy can prevent unstable lateral and directional vehicle behaviour in slow velocity low friction and high velocity high friction conditions. By thoughtfully implementing the controller, different combinations of control strategies are obtainable without ever re-exporting a modified controller. This method of implementation grants great versatility in managing the use of available handling focussed systems and changing the response from the control strategy.

A sensitivity analysis shows that the proposed controls strategy is most susceptible to the road friction estimate that grants the system dynamic road condition perception. Furthermore, the controller shows susceptibility to variation in the CG location along the longitudinal axis of the vehicle. The control strategy however shows complete robustness against variations in vehicle mass and platform noise measured by system sensors. The strategy is also robust against exaggerated magnitudes of sideslip angle noise.

General recommendations for improvements upon this research include coupling the non-linear longitudinal and lateral tyre dynamics within the prediction model to enable brake torque determination by the optimisation problem. Additionally, including the expected actuation delays within the prediction model to obtain oscillatory free control responses and

improve the accuracy of the prediction model. Finally, inclusion of a steering angle predictor or estimator to improve the manoeuvre prediction accuracy over the preview horizon.

References

Abe, M. 2015. Chapter 3 - Fundamentals of Vehicle Dynamics. *In:* ABE, M. (ed.) *Vehicle Handling Dynamics (Second Edition).* Butterworth-Heinemann.

Alipour, H., Bannae Sharifian, M.B. & Sabahi, M. 2014. A modified integral sliding mode control to lateral stabilisation of 4-wheel independent drive electric vehicles. *Vehicle System Dynamics,* 52**,** 1584-1606.

Bosch, H.-R.B., Hamersma, H.A. & Els, P.S. 2016. Parameterisation, validation and implementation of an all-terrain SUV FTire tyre model. *Journal of Terramechanics,* 67**,** 11-23.

Cairano, S.D., Tseng, H.E., Bernardini, D. & Bemporad, A. 2013. Vehicle Yaw Stability Control by Coordinated Active Front Steering and Differential Braking in the Tire Sideslip Angles Domain. *IEEE Transactions on Control Systems Technology,* 21**,** 1236-1248.

Chen, W., Xiao, H., Wang, Q. & Zhao, L. 2016. *Integrated vehicle dynamics and control,* Singapore ;, Wiley.

Cronjé, P.H. & Els, P.S. 2010. Improving off-road vehicle handling using an active anti-roll bar. *Journal of Terramechanics,* 47**,** 179-189.

Ding, S., Liu, L. & Zheng, W.X. 2017. Sliding Mode Direct Yaw-Moment Control Design for In-Wheel Electric Vehicles. *IEEE Transactions on Industrial Electronics,* 64**,** 6752-6762.

European Commision 2009. REGULATION (EC) No 661/2009. Official Journal of the European Union.

European Commision 2018. Advanced driver assistance systems. European Commision, Directorate General for Transport.

Falcone, P., Eric Tseng, H., Borrelli, F., Asgari, J. & Hrovat, D. 2008. MPC-based yaw and lateral stabilisation via active front steering and braking. *Vehicle System Dynamics,* 46**,** 611-628.

Gillespie, T.D. 1992. *Fundamentals of vehicle dynamics,* Warrendale, PA, Society of Automotive Engineers.

International Organization for Standardization 1999. Road vehicles : test procedure for a severe lane-change manoeuvre. *ISO/TR ; 3888.*

Ji, Y., Guo, H. & Chen, H. Integrated control of active front steering and direct yaw moment based on model predictive control. The 26th Chinese Control and Decision Conference (2014 CCDC), 31 May-2 June 2014 2014. 2044-2049.

Lapapong, S. & Brennan, S.N. Terrain-aware rollover prediction for ground vehicles using the zero-moment point method. Proceedings of the 2010 American Control Conference, 30 June-2 July 2010 2010. 1501-1507.

Linström, B.V., Els, P.S. & Botha, T.R. 2018. A real-time non-linear vehicle preview model. *International Journal of Heavy Vehicle Systems,* 25**,** 1-22.

Massera, C.M. & Wolf, D. 2015. *Driver Assistance Controller for Tire Saturation Avoidance up to the Limits of Handling*.

Metzler, M., Tavernini, D., Sorniotti, A. & Gruber, P. An Explicit Nonlinear MPC Approach to Vehicle Stability Control. The 14th International Symposium on Advanced Vehicle Control (AVEC'18), 2018 Beijing, China. Tsinghua University.

Mirzaei, M. 2010. A new strategy for minimum usage of external yaw moment in vehicle dynamic control system. *Transportation Research Part C: Emerging Technologies,* 18**,** 213-224.

National Highway Traffic Safety Administration 2007. Final Regulatory Impact Analysis: Electronic Stability Control Systems. *In:* TRANSPORT, U. S. D. O. (ed.). National Highway Traffic Safety Administration.

National Highway Traffic Safety Administration 2015. Critical Reasons for Crashes Investigated in the National Motor Vehicle Crash Causation Survey. *In:* TRANSPORT, U. S. D. O. (ed.). National Highway Traffic Safety Administration.

Pacejka, H.B. & Bakker, E. 1992. THE MAGIC FORMULA TYRE MODEL. *Vehicle System Dynamics,* 21**,** 1-18.

Quirynen, R., Vukov, M., Zanon, M. & Diehl, M. 2015. Autogenerating microsecond solvers for nonlinear MPC: A tutorial using ACADO integrators. *Optimal Control Applications and Methods,* 36**,** 685-704.

Rajamani, R. 2012. Electronic Stability Control. *In:* RAJAMANI, R. (ed.) *Vehicle Dynamics and Control*. Boston, MA: Springer US.

Ren, B., Chen, H., Zhao, H. & Yuan, L. 2016. MPC-based yaw stability control in in-wheel-motored EV via active front steering and motor torque distribution. *Mechatronics,* 38**,** 103-114.

Siampis, E., Velenis, E., Gariuolo, S. & Longo, S. 2018. A Real-Time Nonlinear Model Predictive Control Strategy for Stabilization of an Electric Vehicle at the Limits of Handling. *IEEE Transactions on Control Systems Technology,* 26**,** 1982-1994.

Siampis, E., Velenis, E. & Longo, S. 2015. Rear wheel torque vectoring model predictive control with velocity regulation for electric vehicles. *Vehicle System Dynamics,* 53**,** 1555-1579.

Thoresson, M.J., Uys, P.E., Els, P.S. & Snyman, J.A. 2009. Efficient optimisation of a vehicle suspension system, using a gradient-based approximation method, Part 1: Mathematical modelling. *Mathematical & Computer Modelling,* 50.

Uys, P.E., Els, P.S., Thoresson, M.J., Voigt, K.G. & Combrinck, W.C. 2006. Experimental determination of moments of inertia for an off-road vehicle in a regular engineering laboratory. *International Journal of Mechanical Engineering Education,* 34**,** 291-300,302-310,312-314.

Yoon, J., Cho, W., Koo, B. & Yi, K. 2009. Unified Chassis Control for Rollover Prevention and Lateral Stability. *IEEE Transactions on Vehicular Technology,* 58**,** 596-609.

Zanelli, A., Domahidi, A., Jerez, J. & Morari, M. 2020. FORCES NLP: an efficient implementation of interior-point methods for multistage nonlinear nonconvex programs. *International Journal of Control,* 93**,** 13-29.

Zheng, S., Zhang, B., Li, S., Wang, G., Zhu, X., Zhu, F. & Lu, X. Model predictive control based vehicle stability control via active front steering. 2017 Chinese Automation Congress (CAC), 20-22 Oct. 2017 2017. 4660-4665.

Rajamani, R., Piyabongkarn, N., Lew, J., Yi, K. and Phanomchoeng, G., 2010. Tire-road friction-coefficient estimation. *IEEE Control Systems Magazine*, *30*(4), pp.54-69.

Khaleghian, S., Emami, A. and Taheri, S., 2017. A technical survey on tire-road friction estimation. *Friction*, *5*(2), pp.123-146.